Wavelets and warping PS seismic images

Chris Graziano & Dave Hale
Center for Wave Phenomena, Colorado School of Mines, Golden CO 80401, USA

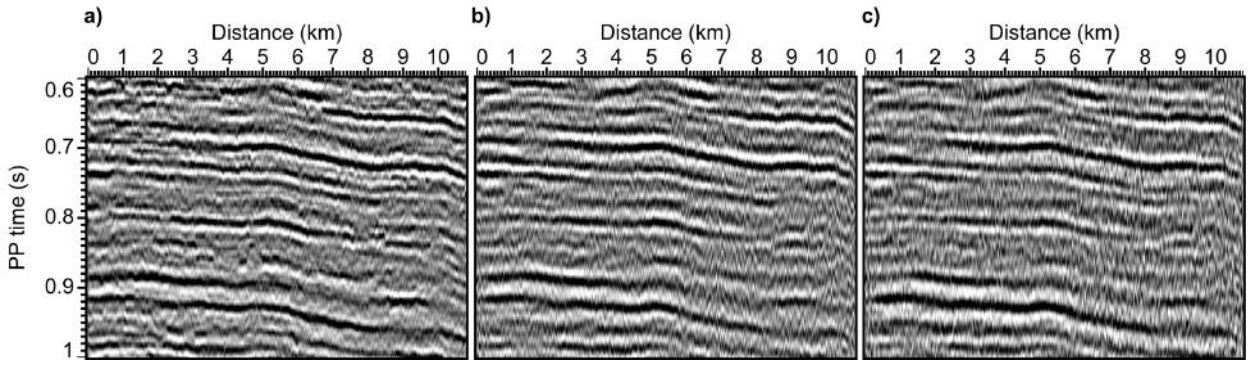

Figure 1. Subsets of a PP image (a), a PS image warped using time shifts and wavelets computed to minimize wavelet distortion caused by warping (b), and a PS image warped using only time shifts (c). All images have been scaled for display to have the same rms amplitude.

ABSTRACT
The process of warping a PS seismic image to align reflectors with those in a PP seismic image can cause wavelet distortion. This distortion can be reduced by deconvolving the PS wavelet from the PS image, warping to PP time, and then convolving with the PP wavelet. Moreover, this *warping-with-wavelets* algorithm can be used to estimate the required PS and PP wavelets. The primary difference between this new algorithm and previous methods is deconvolution of the PS wavelet before warping the PS image to PP time.

Key words: seismic image wavelet warping PP-PS registration

1 INTRODUCTION

Multicomponent data provide a different way to image the subsurface. For example, amplitude and phase differences between PP and PS data can be used to estimate subsurface properties (Garotta et al., 2002; Veire and Landrø, 2006). Before analyzing these differences, we often first compensate for traveltime differences.

The process of warping (squeezing) a PS image to PP time distorts the seismic wavelet (Bansal and Matheney, 2010; Gaiser et al., 2011, 2013; Ursenbach et al., 2013). If the required amount of squeezing varies in space or time, then the warped PS wavelet will also vary. The resulting nonstationary warped PS wavelet can cause errors in inversions for subsurface properties such as density and P- and S-wave velocities (Jing and Rape, 2004; Veire and Landrø, 2006; Khare and Rape, 2007; Bansal and Matheney, 2010).

A proposed solution to this problem of varying PS wavelet distortion has been to design a filter, for each time, that shapes the distorted PS wavelet to a single desired stationary PS wavelet (Bansal and Matheney, 2010). To design the necessary shaping filters, the original wavelet in the PS image must be extracted. Bansal and Matheney (2010) do not describe the wavelet extraction process, but given the original PS wavelet and the amount of squeezing, they compute a squeezed wavelet. The spectrum of the appropriate shaping filter is calculated by dividing the spectrum of the desired stationary PS wavelet by the spectrum of the squeezed wavelet. Applying time- and space-varying shaping filters computed in this way removes wavelet distortion from the squeezed PS image.

Another method of correcting wavelet distortion is proposed by Gaiser et al. (2011). This method uses non-stationary linear filters to modify the S-wave periods of warped PS-waves to match the periods of P-waves. This modification causes the warped PS-waves to resemble S-waves that have been transformed to P-wave time. Gaiser et al. (2011) point out that this method is able to better match the PS-wave data with the P-wave data than if only warping was applied, but wavelet distortions occur because the average V_p/V_s ratios are assumed to be constant over the time of the wavelet. Gaiser et al. (2013) remove this assumption to reduce wavelet distortion and apply filters that compress PS wavelets to yield results similar to those in Gaiser et al. (2011).

The common step to correct wavelet distortion in the previously proposed solutions is to apply a filter after warping the PS image to PP time. We propose a different solution that includes deconvolving the PS wavelet before warping, based on the observation that the problem of wavelet distortion would not exist if the wavelet was an impulse. Moreover, our warping-with-wavelets solution provides a method for estimating the required PS wavelet.

In this paper we first describe the warping-with-wavelets algorithm designed to reduce wavelet distortion. We then describe how wavelet-estimation is possible with this algorithm. Finally, we apply a variant of this algorithm to PP and PS images.

2 WARPING WITHOUT DISTORTION

Suppose that the wavelet in a seismogram is a delta function $\delta(t)$. Figures 2a and 2b represent two simple synthetic seismograms:

$$\begin{aligned} p(t) &= \delta(t-t_1) - \delta(t-t_2), \\ q(t) &= \delta(t-2t_1) - \delta(t-2t_2), \end{aligned} \tag{1}$$

such that

$$p(t) = 2q(2t). \tag{2}$$

Equation 2 is a special case of a more general relationship,

$$p(t) = u'(t)q(u(t)), \tag{3}$$

where $u(t)$ is the mapping from time in $q(t)$ to time in $p(t)$. The amplitude scaling by $u'(t)$ in equations 2 and 3 is necessary because of the squeezing of the impulsive wavelet $\delta(t) = 2\delta(2t)$. Notice that the sequence $2q(2t)$ displayed in Figure 2c exhibits no wavelet distortion.

Let us now consider a non-impulsive wavelet $h(t)$ with Z transform

$$H(z) = \frac{1-0.95z}{(1-1.75z+0.82z^2)(1-1.32z^{-1}+0.82z^{-2})} \tag{4}$$

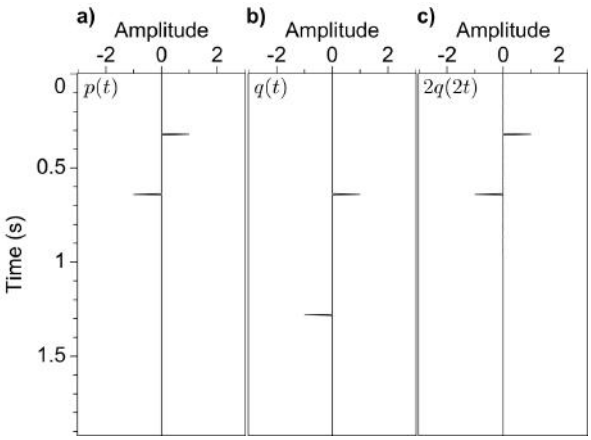

Figure 2. Impulsive sequences $p(t)$ (a) and $q(t)$ (b) to be aligned by warping. The relationship between $p(t)$ and $q(t)$ is $p(t) = 2q(2t)$. Using the known time shifts to warp $q(t)$ to be aligned with $p(t)$ yields no wavelet distortion (c).

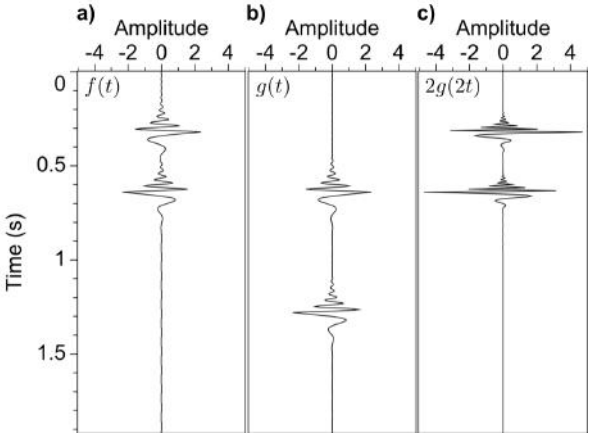

Figure 3. Sequences $f(t)$ (a) and $g(t)$ (b) to be aligned. Both $f(t)$ and $g(t)$ have the same mixed-phase wavelet $h(t)$. Simply warping $g(t)$ to $2g(2t)$ (c) causes wavelet distortion.

and synthetic seismograms computed by convolving this wavelet with the sequences of impulses:

$$\begin{aligned} f(t) &= h(t) * p(t), \\ g(t) &= h(t) * q(t). \end{aligned} \tag{5}$$

This convolution with the wavelet $h(t)$ complicates the relationship between $f(t)$ (Figure 3a) and $g(t)$ (Figure 3b), so that $f(t) \neq 2g(2t)$ (Figure 3c). Figure 3 illustrates that, where the wavelet is not an impulse, simply warping one trace to align with another trace will distort the wavelet. The examples in Figures 2 and 3 suggest that deconvolution of the wavelet should be performed before warping. That is, letting $a(t)$ denote the inverse of the wavelet $h(t)$ such that $a(t)*h(t) = \delta(t)$, we should (1) convolve with $a(t)$, (2) warp, and (3) convolve with $h(t)$. We call this process *warping-with-wavelets*.

2.1 Linear Operators

The sampled wavelet $h(t)$, inverse wavelet $a(t)$, and sequences $f(t)$ and $g(t)$ can be represented by column vectors **h**, **a**, **f**, and **g**, respectively. For illustration, let us suppose that the inverse wavelet **a** has three coefficients (a_0, a_1, a_2), such that convolution of **a** with **g** is represented by

$$\mathbf{Ag} = \begin{bmatrix} a_0 & 0 & 0 & 0 & 0 \\ a_1 & a_0 & 0 & 0 & 0 \\ a_2 & a_1 & a_0 & 0 & 0 \\ 0 & a_2 & a_1 & a_0 & 0 \\ 0 & 0 & a_2 & a_1 & a_0 \end{bmatrix} \begin{bmatrix} g_0 \\ g_1 \\ g_2 \\ g_3 \\ g_4 \end{bmatrix}, \tag{6}$$

or, equivalently,

$$\mathbf{Ga} = \begin{bmatrix} g_0 & 0 & 0 \\ g_1 & g_0 & 0 \\ g_2 & g_1 & g_0 \\ g_3 & g_2 & g_1 \\ g_4 & g_3 & g_2 \end{bmatrix} \begin{bmatrix} a_0 \\ a_1 \\ a_2 \end{bmatrix}. \tag{7}$$

Note that columns of **A** contain only delayed copies of **a** and columns of **G** contain only delayed copies of **g**, so that both **A** and **G** are Toeplitz matrices. Also recall that convolution is commutative; $\mathbf{Ag} = \mathbf{Ga}$. Convolution of the inverse wavelet **a** with **g** is equivalent to deconvolution of the wavelet **h** from **g**.

Warping is defined by the linear operator **S**. If one squeezes **g**, the frequency spectrum of **g** is stretched, which could cause aliasing. Therefore, before squeezing, we apply a low-pass filter to **g** to attenuate frequencies that would otherwise be aliased after warping. We include this low-pass anti-alias filter in the warping operator **S**. The result of applying **S** to **Ag** is a vector **SAg** containing the warped result of deconvolving wavelet **h** from **g**. Because **S** is a time-varying operator, it does not commute with **A**; $\mathbf{SA} \neq \mathbf{AS}$. The final step in our warping-with-wavelets algorithm is to convolve **h** with **SAg** so that

$$\mathbf{f} = \mathbf{HSAg}. \tag{8}$$

Figure 4 shows that wavelet distortion is reduced by using this algorithm to warp $g(t)$ to $f(t)$. Note that, although $\mathbf{HA} = \mathbf{I}$, $\mathbf{f} = \mathbf{HSAg} \neq \mathbf{HASg} = \mathbf{Sg}$, because **S** and **A** do not commute. In other words, as illustrated in Figure 4, $\mathbf{f} \neq \mathbf{Sg}$; warping alone is inadequate.

3 ESTIMATING THE WAVELET

To warp seismic traces without wavelet distortion, the wavelet **h**, or equivalently, its inverse **a**, must be known. Let us now consider how we might use equation 8 to estimate **a** and, hence, **h**.

Multiplying both sides of equation 8 by **A**, we obtain

$$\mathbf{Af} = \mathbf{SAg}. \tag{9}$$

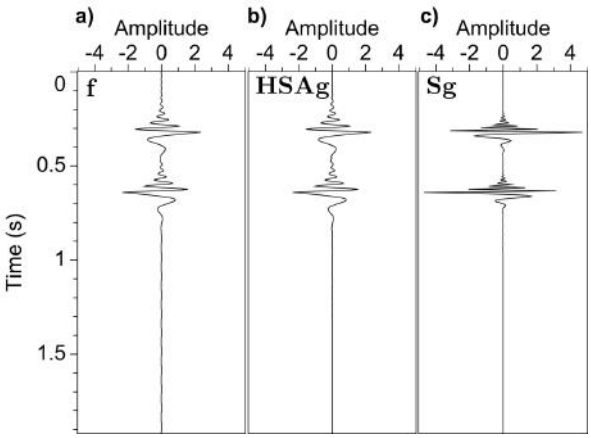

Figure 4. The sequence **f** (a), the sequence **HSAg** (b) obtained using the warping-with-wavelets algorithm, and the sequence **Sg** (c) obtained using only warping.

Because convolution is commutative, we can rewrite equation 9 as

$$\mathbf{Fa} = \mathbf{SGa}, \tag{10}$$

or

$$\mathbf{Fa} - \mathbf{SGa} = \mathbf{0}. \tag{11}$$

Now define $\mathbf{D} \equiv \mathbf{F} - \mathbf{SG}$, so that

$$\mathbf{Da} = \mathbf{0}. \tag{12}$$

The number of columns in **D** equals the number of unknown coefficients in the inverse wavelet **a**, so for coefficients (a_0, a_1, a_2) we have

$$\mathbf{D} = \begin{bmatrix} \mathbf{d}_0 & \mathbf{d}_1 & \mathbf{d}_2 \end{bmatrix}, \tag{13}$$

where

$$\begin{aligned} \mathbf{d}_0 &= \mathbf{f}_0 - \mathbf{Sg}_0, \\ \mathbf{d}_1 &= \mathbf{f}_1 - \mathbf{Sg}_1, \\ \mathbf{d}_2 &= \mathbf{f}_2 - \mathbf{Sg}_2. \end{aligned} \tag{14}$$

Here, $\mathbf{f}_0$ is simply **f**, $\mathbf{f}_1$ is **f** delayed by one sample, and $\mathbf{f}_2$ is **f** delayed by two samples. Likewise, $\mathbf{g}_0$ is simply **g**, $\mathbf{g}_1$ is **g** delayed by one sample, and $\mathbf{g}_2$ is **g** delayed by two samples. Notice that in computing the matrix **D**, the warping operator **S** is applied multiple times to different delayed versions of **g**.

The trivial solution to equation 12 is $\mathbf{a} = \mathbf{0}$. We eliminate this solution by setting the coefficient $a_0 = 1$. We could set a_0 to any value, but this would only scale the coefficients of the wavelet **h** by a_0. Using equation 12 alone, the true amplitudes of **h** and **a** cannot be recovered; only their shapes can be estimated. With $a_0 = 1$, equation 12 becomes

$$\begin{bmatrix} \mathbf{d}_1 & \mathbf{d}_2 \end{bmatrix} \begin{bmatrix} a_1 \\ a_2 \end{bmatrix} = -\mathbf{d}_0. \tag{15}$$

In equation 15, we have as many equations as time

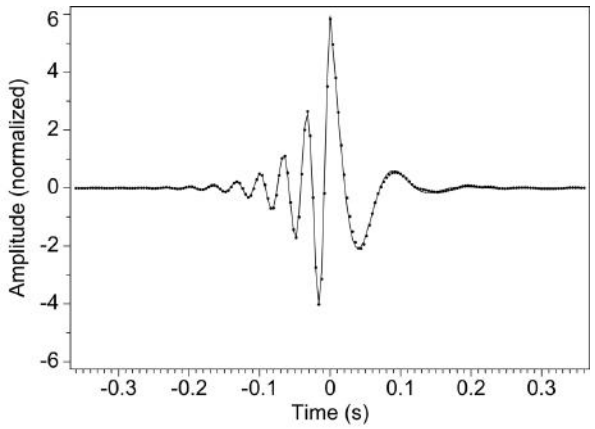

Figure 5. The known wavelet (solid curve) and the estimated wavelet (dots).

samples in $\mathbf{f}$ and $\mathbf{g}$, but only two unknowns a_1 and a_2, which leads us to use the least-squares method and minimize $\|\mathbf{d}_0 + a_1\mathbf{d}_1 + a_2\mathbf{d}_2\|_2$. To compute a_1 and a_2, we solve the normal equations obtained by multiplying both sides of equation 15 by $[\mathbf{d}_1\ \mathbf{d}_2]^\intercal$:

$$\begin{bmatrix} \mathbf{d}_1^\intercal\mathbf{d}_1 & \mathbf{d}_1^\intercal\mathbf{d}_2 \\ \mathbf{d}_2^\intercal\mathbf{d}_1 & \mathbf{d}_2^\intercal\mathbf{d}_2 \end{bmatrix} \begin{bmatrix} a_1 \\ a_2 \end{bmatrix} = \begin{bmatrix} -\mathbf{d}_1^\intercal\mathbf{d}_0 \\ -\mathbf{d}_2^\intercal\mathbf{d}_0 \end{bmatrix}. \tag{16}$$

The leftmost matrix in equation 16 is not Toeplitz because the matrix $\mathbf{S}$ is a time-varying operator that is applied to delayed copies of $\mathbf{g}$. This matrix is however symmetric positive semidefinite, which enables us to solve equation 16 by Cholesky decomposition. A similar system of equations can be obtained for any number of coefficients in the inverse wavelet $\mathbf{a}$, which need not be causal.

After estimating the inverse wavelet $\mathbf{a}$, we easily recover the wavelet $\mathbf{h}$ as the filter that shapes the inverse wavelet $\mathbf{a}$ to a unit impulse (e.g., Robinson and Treitel, 2000). Then, with the estimated $\mathbf{h}$ and $\mathbf{a}$, we can apply the warping-with-wavelets algorithm; that is, we can compute $\mathbf{HSAg}$.

We tested this wavelet-estimation process using the sequences $\mathbf{f}$ and $\mathbf{g}$ displayed in Figures 3a and 3b, respectively. We chose to estimate large numbers of coefficients in the inverse wavelet $\mathbf{a}$ and the wavelet $\mathbf{h}$, which were 81 and 181, respectively, because in this example the known wavelet and its inverse are both infinitely long. (Recall equation 4.) Figure 5 shows that the estimated wavelet is nearly identical to the known wavelet. However, it is important to recall that for this simple example, the wavelet in $\mathbf{f}$ is identical to that in $\mathbf{g}$.

4 APPLICATION TO PP-PS IMAGES

To estimate wavelets and to reduce wavelet distortion caused by warping a PS image (Figure 6b) to a PP image (Figure 6a), a modification of the warping-with-wavelets algorithm described above is required. Wavelets in PP and PS images are unlikely to be identical, in part, because attenuation often affects S-waves more than it does P-waves (Ursenbach et al., 2013). This difference leads us to use an estimated inverse PS wavelet $\mathbf{a}$ to deconvolve the PS wavelet from the PS image, allowing us to warp the resulting image to PP time without wavelet distortion. Although the presence of noise in the PS image will prevent us from completely deconvolving the PS wavelet from the PS image, we show below an example of reduced wavelet distortion in the presence of noise. Then, after we warp the deconvolved PS image, we convolve with the estimated PP wavelet $\mathbf{h}$ to obtain a PS image with a PP wavelet. Ideally, remaining differences in the two images should be due to differences in PP and PS reflectivity.

Before estimating the PS inverse wavelet $\mathbf{a}$ and the PP wavelet $\mathbf{h}$ and applying the warping-with-wavelets algorithm, we first apply a time-varying gain to the PP and PS images displayed in Figures 6a and 6b, respectively, so that PP and PS amplitudes are comparable. Let the PP and PS images be represented by column vectors $\mathbf{f}$ and $\mathbf{g}$, respectively. We found the time shifts used to warp the PS image $\mathbf{g}$ to the PP image $\mathbf{f}$ by smooth dynamic warping (Hale and Compton, 2013) and this warping of $\mathbf{g}$ to $\mathbf{f}$ is again represented by the linear operator $\mathbf{S}$.

In equation 8 we have two unknown sequences, $\mathbf{h}$ and $\mathbf{a}$; and if $\mathbf{HA}\neq\mathbf{I}$, then we cannot eliminate the unknown wavelet $\mathbf{h}$ by simply multiplying both sides of equation 8 by $\mathbf{A}$. Instead of solving for both $\mathbf{h}$ and $\mathbf{a}$ simultaneously, we iteratively compute one and then the other.

We begin this iterative process by letting $\mathbf{a} = \boldsymbol{\delta}$. We then compute $\mathbf{q} = \mathbf{Sg}$, which simplifies equation 8 to

$$\mathbf{f} = \mathbf{Hq}, \tag{17}$$

or, equivalently,

$$\mathbf{f} = \mathbf{Qh}, \tag{18}$$

where columns of the matrix $\mathbf{Q}$ contain delayed copies of $\mathbf{q}$.

In equation 18, we have as many equations as we have samples in the PP and PS images $\mathbf{f}$ and $\mathbf{g}$, and we have a significantly smaller number of unknown PP wavelet coefficients in $\mathbf{h}$. The relatively small number of unknowns leads us to compute $\mathbf{h}$ using the least-squares method to minimize $\|\mathbf{f}-\mathbf{Qh}\|_2$. Specifically, we solve the normal equations obtained by multiplying both sides of the equation 18 by $\mathbf{Q}^\intercal$:

$$\mathbf{Q}^\intercal\mathbf{Qh} = \mathbf{Q}^\intercal\mathbf{f}. \tag{19}$$

The matrices $\mathbf{Q}$, $\mathbf{Q}^\intercal$, and $\mathbf{Q}^\intercal\mathbf{Q}$ are Toeplitz because columns of $\mathbf{Q}$ contain delayed copies of $\mathbf{q}$. Therefore, the resulting PP wavelet $\mathbf{h}$ is a filter that shapes the warped

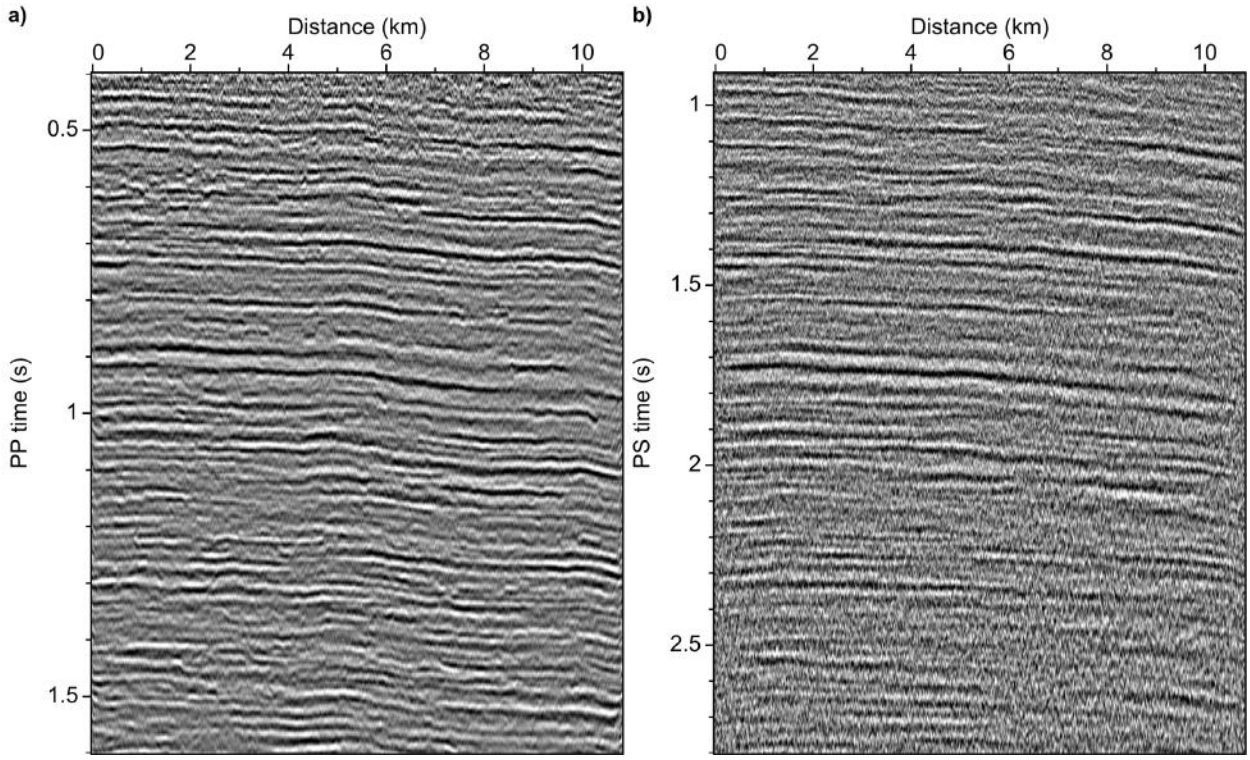

Figure 6. A subset of a PP image (a) and a roughly corresponding subset of a PS image (b). Note the differences in PP and PS time scales.

PS image $\mathbf{q}$ to match the PP image $\mathbf{f}$. In other words, the estimated PP wavelet $\mathbf{h}$ is similar to the shaping filters designed by Bansal and Matheney (2010), but here is time-invariant. At this point, we have completed one iteration.

We then use the estimated PP wavelet $\mathbf{h}$ to compute $\mathbf{P} = \mathbf{HSG}$, which reduces equation 8 to

$$\mathbf{f} = \mathbf{Pa}. \tag{20}$$

In equation 20, we again have as many equations as samples in the PP and PS images $\mathbf{f}$ and $\mathbf{g}$ and a significantly smaller number of unknown inverse PS wavelet coefficients in $\mathbf{a}$. The relatively small number of unknowns compared to equations again leads us to use the least-squares method and minimize $\|\mathbf{f} - \mathbf{Pa}\|_2$. That is, we solve the normal equations obtained by multiplying both sides of equation 20 by $\mathbf{P}^\mathsf{T}$:

$$\mathbf{P}^\mathsf{T}\mathbf{Pa} = \mathbf{P}^\mathsf{T}\mathbf{f}. \tag{21}$$

Here the matrices $\mathbf{P}$, $\mathbf{P}^\mathsf{T}$, and $\mathbf{P}^\mathsf{T}\mathbf{P}$ are not Toeplitz because the time-varying operator $\mathbf{S}$ in $\mathbf{P} = \mathbf{HSG}$ is applied to all delayed copies of $\mathbf{g}$ in the columns of $\mathbf{G}$. Therefore, we compute the PS inverse wavelet $\mathbf{a}$ using Cholesky decomposition of $\mathbf{P}^\mathsf{T}\mathbf{P}$, instead of using faster solvers appropriate for Toeplitz matrices. Notice, in equation 20, that if we multiply the PP wavelet $\mathbf{h}$ by a constant and divide the estimated inverse PS wavelet $\mathbf{a}$ by the same constant, then the matrix on the right-hand side will be unchanged, which means that only the shape of the inverse PS wavelet $\mathbf{a}$ can be recovered, not its true amplitudes. This same logic can be applied to equation 18 (where we are solving for the PP wavelet $\mathbf{h}$), meaning that only the shape of the PP wavelet $\mathbf{h}$ can be recovered, not its true amplitudes.

We next use equation 18 to compute an updated PP wavelet $\mathbf{h}$; but, instead of using the inverse PS wavelet $\mathbf{a} = \boldsymbol{\delta}$, we use the most recent estimate of $\mathbf{a}$. We then compute $\mathbf{q} = \mathbf{SAg}$ and solve equation 19 for an updated PP wavelet $\mathbf{h}$. At this point, we have completed two iterations. We can repeat this iterative process for any number of iterations, but in the examples below we use 11 iterations.

The PP wavelet $\mathbf{h}$ and the PS wavelet corresponding to the inverse PS wavelet $\mathbf{a}$ estimated in the first iteration are shown in Figures 7a and 7b, respectively. After only one iteration, the PS wavelet is an impulse because the inverse PS wavelet $\mathbf{a}$ is initialized to be an impulse $\boldsymbol{\delta}$, which implies that $\mathbf{f} = \mathbf{HSg}$. The PP wavelet $\mathbf{h}$ is a filter that shapes the warped PS image $\mathbf{Sg}$ to the PP image $\mathbf{f}$. If we use the impulse inverse PS wavelet $\mathbf{a} = \boldsymbol{\delta}$ and the estimated PP wavelet $\mathbf{h}$ to implement the modified warping-with-wavelets algorithm, we obtain the warped PS image shown in Figure 9c. The

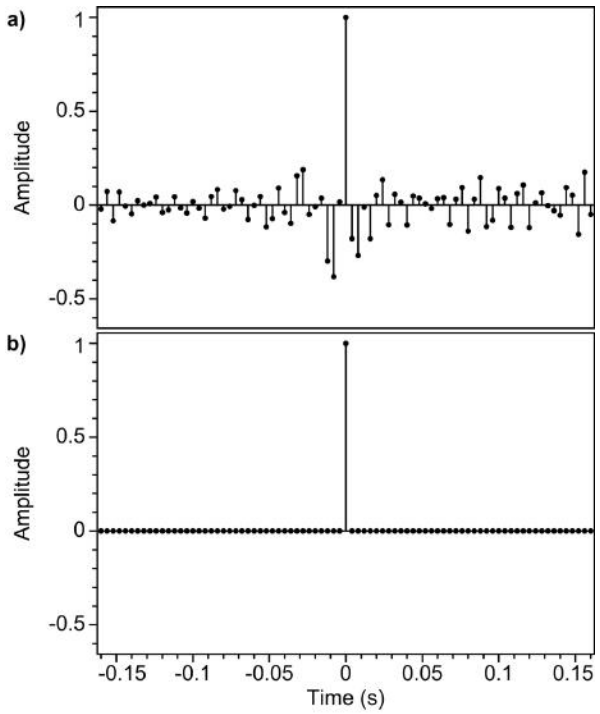

Figure 7. A shaping filter (a) used to shape the warped PS image (Figure 9d) to the PP image (Figure 9a). In this case, the PS wavelet is not estimated and is assumed to be a unit impulse (b).

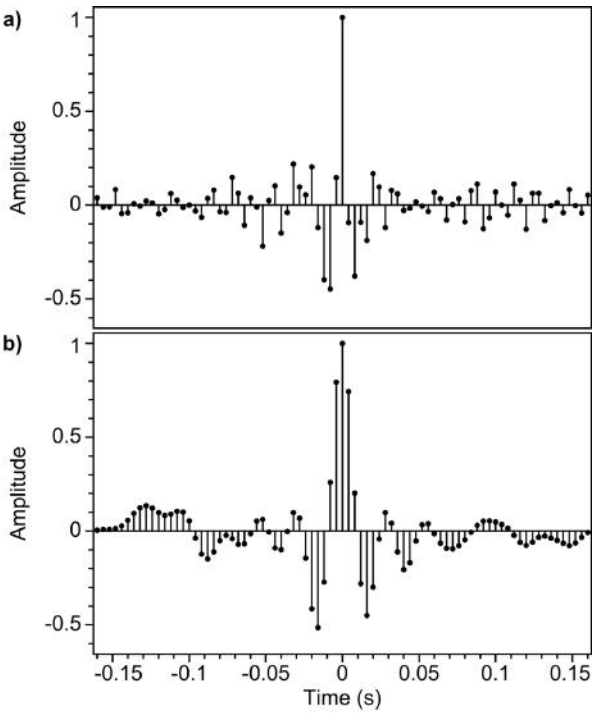

Figure 8. The estimated PP wavelet (a) and the estimated PS wavelet (b) after 11 iterations.

resulting rms (root-mean-square) difference between **f** and **HSAg** is 0.672.

After 11 iterations, we obtain the PP wavelet **h** and PS wavelet (corresponding to the estimated inverse PS wavelet **a**) shown in Figures 8a and 8b, respectively. Figure 9b displays the image **HSAg** computed using the modified warping-with-wavelets algorithm, with the estimated inverse PS wavelet **a** and PP wavelet **h**. The rms difference between **f** and **HSAg** is 0.666, which is slightly smaller than the rms difference between **f** and **HSAg** after only one iteration. Here, we stopped after 11 iterations in the wavelet-estimation process, when the rate of decrease in the rms difference between **f** and **HSAg** was less than 0.00005 per iteration.

5 DISCUSSION

Although the inverse PS wavelet **a** and PP wavelet **h** obtained after one and 11 iterations differ significantly, the results of using the modified warping-with-wavelets algorithm for one (**HSg**) and 11 (**HSAg**) iterations are similar (Figures 9c and 9b, respectively). **HSAg** and **HSg** are more similar to **f** (Figure 9a) than is **Sg** (Figure 9d), due to a reduction in wavelet distortion in both **HSAg** and **HSg**. In the shallow portions of **HSAg** and **HSg**, highlighted by the black rectangles in Figures 9b and 9c, **HSAg** differs somewhat from **HSg** because the amount of squeezing applied by **S** varies most rapidly there. The small reduction (0.672 to 0.666) in rms differences of **f** compared to **HSg** and **f** compared to **HSAg** may be a result of only this small portion of the warped PS image having varying squeezing.

In any case, a single shaping filter cannot shape **Sg** to **f**. Stewart et al. (2002) observe that PP and PS waves often have different reflection coefficients. This difference in reflection coefficients is part of the reason why the estimated PP wavelet (shaping filter) **h** cannot shape $\mathbf{q} = \mathbf{SAg}$ to exactly equal **f** as shown in equation 18. Indeed, in warping with wavelets we seek to preserve any differences in reflection coefficients.

However, the PP wavelet **h** does reduce noise in warped images **HSAg** (Figure 9b) and **HSg** (Figure 9c) because the PP image has less noise than the PS image and the PP wavelet **h** will match the noisy **HSg** or **HSAg** to the less noisy PP image **f**.

In our modified warping-with-wavelets example, we estimated one inverse PS wavelet **a** and one PP wavelet **h** for the PS and PP images, which implies that we assumed that these wavelets do not vary in time or space. However, we could modify the warping-with-wavelets algorithm to estimate multiple wavelets as a function of time and space. Whether we estimate one wavelet or multiple wavelets, the key is to deconvolve the wavelet in the PS image before warping that image.

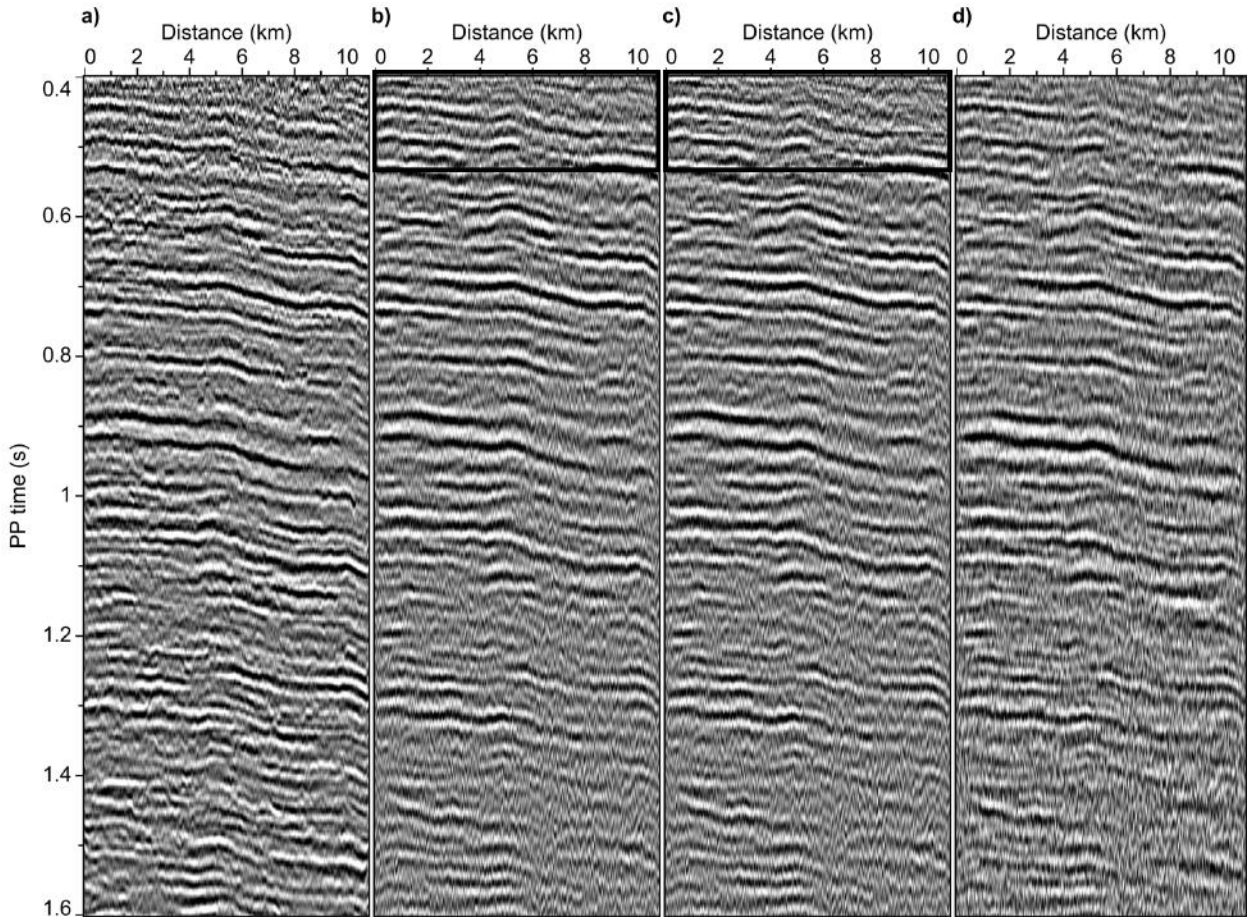

Figure 9. A PP image (a) with PS images obtained by three warping methods: the proposed warping-with-wavelets algorithm (b), applying a shaping filter to make the warped PS image look like the PP image (c), and simply warping the PS image (d). All images have been scaled for display to have the same rms amplitude. Black rectangles highlight small differences between (b) and (c).

6 CONCLUSION

Two warping-with-wavelets algorithms are proposed to minimize wavelet distortion caused by warping. One algorithm assumes a single wavelet for both the PP and PS images and the other algorithm assumes different wavelets in those images. In the case of different wavelets, one filter is designed to deconvolve the PS wavelet from the PS image before warping and another filter is designed to convolve the PP wavelet with the warped deconvolved PS image. This process reduces wavelet distortion caused by warping, while yielding estimates of PP and PS wavelets.

ACKNOWLEDGMENTS

This work was supported by the sponsors of the Consortium Project on Seismic Inverse Methods for Complex Structures at the Colorado School of Mines. The seismic PP and PS images shown in Figures 1, 6, and 9 were provided courtesy of Sinopec.

REFERENCES

Bansal, R., and M. Matheney, 2010, Wavelet distortion correction due to domain conversion: Geophysics, **75**, V77–V87.

Gaiser, J., R. Verm, and A. Chaveste, 2011, Extending the high end of C-wave bandwidth to match P-wavelengths: SEG Technical Program Expanded Abstracts, 4334–4338.

———, 2013, Pseudo S-wave broadband response of C-waves after domain change: The Leading Edge, **32**, 50–62.

Garotta, R., P.-Y. Granger, and H. Dariu, 2002, Combined interpretation of PP and PS data provides direct access to elastic rock properties: The Leading Edge, **21**, 532–535.

Hale, D., and S. Compton, 2013, Smooth dynamic warping: CWP Report 764.

Jing, C., and T. Rape, 2004, Resolvability analysis for rock property inversions of multicomponent seismic data: SEG Technical Program Expanded Abstracts, 897–900.

Khare, V., and T. Rape, 2007, Density inversion using joint PP/PS data: Sensitivity to the angle range: SEG Technical Program Expanded Abstracts, 965–969.

Robinson, E. A., and S. Treitel, 2000, Geophysical signal analysis: Society of Exploration Geophysicists.

Stewart, R. R., J. E. Gaiser, R. J. Brown, and D. C. Lawton, 2002, Tutorial converted-wave seismic exploration: Methods: Geophysics, **67**, 1348–1363.

Ursenbach, C., P. Cary, and M. Perz, 2013, Limits on resolution enhancement for PS data mapped to PP time: The Leading Edge, **32**, 64–71.

Veire, H. H., and M. Landrø, 2006, Simultaneous inversion of PP and PS seismic data: Geophysics, **71**, R1–R10.